Received: 31 December 2022 | Revised: 21 June 2023 | Accepted: 30 June 2023

DOI: 10.1002/jex2.101

RESEARCH ARTICLE

Internalization of extracellular vesicles from *Lactobacillus johnsonii* N6.2 elicit an RNA sensory response in human pancreatic cell lines

Danilo R. da Silva | **Claudio F. Gonzalez** | **Graciela Lorca**

Department of Microbiology and Cell Science, Genetics Institute, Institute of Food and Agricultural Sciences, University of Florida, Gainesville, Florida, USA

Correspondence
Graciela Lorca, Department of Microbiology and Cell Science, Genetics Institute, Institute of Food and Agricultural Sciences, University of Florida, Gainesville, Florida, USA.
Email: glorca@ufl.edu

Funding information
National Institute of Diabetes and Digestive and Kidney Diseases, Grant/Award Number: R01DK121130

Abstract

Cells of all domains of life can secrete extracellular vesicles (EV). These secreted vesicles have been indicated as vehicles carrying molecules that facilitate intra- and inter-species interaction. *Lactobacillus johnsonii* N6.2, a bacterium used in probiotic preparations, has been shown to produce nano-sized EV. In the present work we used *L. johnsonii* N6.2 EV, concentrated from exosome-depleted MRS supernatant, to identify the uptake mechanisms of EV and the impact of the RNA cargo in the EV on the upregulation of the cellular response of βlox5 human pancreatic cells. Using eukaryotic uptake inhibitors, it was found that EV are internalized by the clathrin/dynamin mediated endocytosis pathway. Further co-localization experiments with the endosome markers RAB5, RAB7 and LAMP1 as well as calcein indicated that EV escape the endosome shortly after RAB7 fusion. Using the expression of the 2′,5′-oligoadenylate synthetase (OAS) host pathway, previously identified as targeted by *L. johnsonii* EV, we found that the host cellular response to the EV are dependent on the integrity of the external components of the EV as well as on the RNA cargo. Global transcriptome analysis was performed on EV and the bacterial whole cell. It was found that the RNA transcripts found within the EV largely represent the most abundantly transcribed genes in the bacterial cells such as those associated with protein synthesis and glycolysis. Further analysis showed an enrichment of smaller size transcripts as well as those encoding for membrane bound or extracellular proteins in *L. johnsonii*'s EV.

KEYWORDS
2′-5′-oligoadenylate synthetase, endosome, extracellular vesicles, human beta cell line, *Lactobacillus johnsonii* N6.2, nanovesicles, probiotic, βlox5

1 | INTRODUCTION

Membrane-derived vesicles have been found to be an integral part of intra- and inter-species interaction. Eukaryotic extracellular vesicles (EV) have been extensively studied and characterized over the years, and specific mechanisms of EV synthesis and release have been identified (Gandham et al., 2020). These eukaryotic EV can be generated from intracellular membrane compartments and released to the environment by exocytosis, such as exosomes, or from the plasma membrane through budding, such as microvesicles (Pan et al., 1985; Schrier et al., 1971). The intra-species communication is mediated by passive or active mechanisms of EV internalization. In addition, different sensory pathways may be activated depending on the composition of the EV cargo as well as the location of the cargo delivery (Feng et al., 2010; Mathieu et al., 2019). Interestingly, it has been determined that viruses and microorganisms (or their components) enter eukaryotic cells using similar pathways with variable outcomes (Cossart & Helenius, 2014).

Starting with the observation of EV from Gram-negative bacteria in the 1960′s, bacterial EV have increasingly been at the forefront in the study of host:microbe interactions (Chatterjee & Das, 1967) . Bacterial EV were first described to be produced from the outer membrane of Gram-negative bacteria and named outer membrane vesicles (OMV) and widely studied in the context of pathogen/host interactions (Chatterjee & Chaudhuri, 2011; Soult et al., 2013). Likewise, Gram-positive bacteria have been shown to be able to shed EV with the ability to carry pathogenic determinants or antimicrobial peptides (Briaud & Carroll, 2020). For example, *Staphylococcus aureus*-derived EV were shown to induce inflammation in atopic dermatitis, and EV from *Bacillus anthracis* were shown to carry the anthrax toxin. Within lactobacilli, *Lactobacillus acidophilus*-derived EV carry antimicrobial peptides such as bacteriocins as a means to control competing bacterial growth (Dean et al., 2020; Hong et al., 2011; Rivera et al., 2010).

There are many mechanisms by which bacterial-derived EV are internalized by eukaryotic cells. For example, the human macrophage cell line, THP-1, has been shown to interact and internalize *S. aureus* EV by a dynamin-dependent endocytic pathway while *Propionibacterium acnes*-EV are internalized by keratinocytes via clathrin-dependent mechanisms (Choi et al., 2018; Wang et al., 2020). Overall, the mechanism of bacterial EV internalization by non-phagocytic cells suggests that is species specific. As more studies characterized the cargo in the EV produced by the different bacterial species in the context of host interactions, it has been shown that bacterial EV can elicit not only pathogenic but also beneficial/tolerogenic effects on the host. While the largest body of research in bacterial EV has focused on the characterization of the pathogenicity determinant cargo, the characterization of tolerogenic responses induced by beneficial and commensal microorganisms is scarce.

Recently, we have reported the induction of a tolerogenic M2 phenotype in macrophages exposed to *Lactobacillus johnsonii* N6.2 EV (Teixeira et al., 2022). Using scanning electron microscopy, we observed extracellular vesicles produced by *L. johnsonii* N6.2 ranging between 90 and 125 nm in size (formerly named nanovesicles, NV) (Harrison et al., 2021). Untargeted lipidomic and proteomics comparisons of the *L. johnsonii* N6.2 EV and cell membrane fractions, revealed that *L. johnsonii* N6.2 EV are enriched in phospholipids and have a unique protein composition (Harrison et al., 2021). Using these differentially enriched proteins as biomarkers, the host response to *L. johnsonii* N6.2 EV was evaluated in blood samples of volunteers that ingested *L. johnsonii* N6.2. The individuals consuming the whole probiotic showed increased amounts of IgA and IgG for EV or the Sdp protein used as an EV biomarker (Harrison et al., 2021). These results indicated that EV produced by *L. johnsonii* N6.2 in the intestinal tract have the potential to mediate systemic immunomodulatory responses in the host. To evaluate the impact of EV on host responses in the context of diabetes, we analyzed the global transcriptome response of the human pancreatic cell line, βlox5, to *L. johnsonii* N6.2 EV. The addition of EV triggered an intracellular immune response by activating translocation of the aryl hydrocarbon receptor (AHR) and upregulating RNA sensing and degradation genes (Teixeira et al., 2022). The modulation of RNA sensing genes is in agreement with our previous report where we found that whole bacteria or cell-free extracts induced the expression of nucleic acid sensing receptors such as TLR7 and TLR9 (Kingma et al., 2011). Interestingly, EV stimulation also prevented cytokine induced apoptosis in βlox5 cells in vitro (Teixeira et al., 2022).

Based on these findings, we hypothesized that *L. johnsonii* N6.2-derived EV require active internalization mechanisms to mediate an RNA-dependent immune response on host cell. In this report, we evaluated the internalization mechanism and transit pathways of EV using human pancreatic cell lines. Furthermore, analysis of the RNA component found within the EV showed to be essential in triggering an RNA sensing response by inducing the expression of the 2′-5′-Oligoadenylate Synthetase pathway.

2 | MATERIALS AND METHODS

2.1 | Bacterial growth and EV isolation

L. johnsonii N6.2 was grown in exosome depleted de Man, Rogosa, Sharpe media (ED-MRS) media at 37°C under static condition as previously described (Harrison et al., 2021; Valladares et al., 2010). For vesicle isolation the *L. johnsonii* N6.2 was activated twice prior to inoculation in 500 mL of ED-MRS. The *L. johnsonii* N6.2 was grown to an optical density (OD) of 1 at 600 nm. The bacterial cells were pelleted by centrifugation at 4°C for 20 min at 15,900 × *g*. The supernatant was then filtered through a 0.2 μm aPES filter to remove any remaining cells and larger bacterial cellular debris. The filtered supernatant was then ultracentrifuged at 4°C for 2 h at 175,000 × *g*. The EV pellet was washed twice with PBS (137 mM NaCl, 2.7 mM KCl, 10 mM Na_2HPO_4, 1.8 mM KH_2PO_4) and resuspended in 500 μL of PBS or βlox5 media. The vesicles suspended in PBS were subsequently quantified using a NanoSight 300 (Malvern Instruments Ltd, Malvern, UK) at the University of Florida ICBR Flow Core Facility, RRID:SCR_019119.

2.2 | EV staining

For staining, EV were isolated as described above with the following modification. After the first PBS wash the EV pellet was resuspended in 0.1 M $NaHCO_3$ (pH = 8.3) and 33 μL of Alexa Fluor 594 NHS Ester (Succinimidyl Ester) (Thermo Scientific,

Waltham, MA, USA) dissolved in dimethyl sulfoxide (DMSO) (Sigma-Aldrich, Saint Louis, MO, USA) (10 mg/mL) or 1 μL of 4 mM 18:1 lissamine rhodamine B sulfonyl (Avanti Polar Lipids, AL). The EV were incubated at room temperature under gentle shaking for 1 h. The EV were then ultracentrifuged following the previous parameters and rinsed with PBS once before pelleting and resuspending in 500 μL of PBS or βlox5 media.

2.3 | Physicochemical analysis of the EV and βlox5

The EV ζ potential was analyzed with a ZetaSizer Ultra particle analyser (Malvern Instruments, Malvern, UK) at 25°C. EV were isolated with the methods described above and resuspended in PBS. The EV were diluted 10x in filtered H_2O to a final 10% PBS concentration. The βlox5 ζ potential was measured by fixing the cells in 4% paraformaldehyde in PBS for 10 min, then washed in ultrapure H_2O and resuspended 1 mL of ultrapure H_2O. The hydrodynamic ζ average diameter was calculated by the light scattering method, and the ζ potential was determined by applying the Smoluchowski approximation. The electrostatic charge on the surfaces of the EV and βlox5 was characterized as the ζ potential.

2.4 | βlox5 cell line propagation

The pancreatic cell line βlox5 (Halvorsen et al., 1999) was grown in DMEM, Dulbecco's Modified Eagle Medium (DMEM) low glucose (1 g/L) supplemented with 10% heat inactivated FBS (Sigma-Aldrich, Saint Louis, MO, USA), 1% penicillin and streptomycin solution containing 10,000 units of penicillin and 10 mg of streptomycin/ml (Sigma-Aldrich, Saint Louis, MO, USA), 0.2% of BSA, HEPES (15 mM), pH = 7, and 5 mL of MEM non-essential amino acids (Sigma-Aldrich, Saint Louis, MO, USA) and incubated at 37°C with 5% CO_2. For EV uptake assays, βlox5 cells were seeded at 3×10^5 cell 6-well plate or 6-well plate containing poly-D-lysine-coated (Sigma-Aldrich, Saint Louis, MO) coverslips for visualization. Once the βlox5 cells reached 80% confluence ($\sim 1 \times 10^6$) the cells were pre-treated for 1 h with DMSO vehicle control (1.61 μL/mL), chlorpromazine (5 μM), dynasore (80 μM), methyl-β-cyclodextrin (50 μM), cytochalasin D (10 nM) or 5(*N*-ethyl-*N*-isopropyl)-amiloride (4 nM). The cytotoxic effects of each inhibitor on the βlox5 cells were determined by 3-(4,5-dimethylthiazol-2-yl)−2,5-diphenyltetrazolium bromide (MTT) assay (Figure S1) (Wakatsuki et al., 2001). After pre-treatment, the cells were incubated with EV (at a ratio of 10,000:1 EV:cell) in the presence of the inhibitors, either for 1 h with labelled EV for visualization, or for 5 h with native EV for qRT-PCR determinations. After the incubation the cells were prepared for visualization or RNA extraction as detailed below.

2.5 | Fluorescent microscopy

βlox5 cells were grown in 6-well plates containing a poly-D-lysine-coated coverslip. Once cells reached confluence the cells were treated with Alexa 594 labelled EV. The cells were fixed for fluorescent microscopy utilizing a modified immunofluorescence protocol from Nano et al. (2021). Briefly, the media was removed from the cells and rinsed once with PBS and fixed with 4% paraformaldehyde in PBS for 10 min. The fixed cells were rinsed with PBS containing 10 mM glycine and 0.2% sodium azide (PBS-GSA). The cell membrane was labelled with an Alexa 488 - wheat germ agglutinin conjugate (Thermo Scientific, Waltham, MA) for 10 min then fixed again. Then, cells were permeabilized with PBS-GSA containing 0.5% Triton X-100. For immunofluorescence labelling, cells were first blocked for 30 min with a PBS-GSA solution containing 1% BSA. The cells were washed twice with PBS-GSA and incubated for 5 min in the same solution. Next, the following primary antibodies against the endocytosis markers were added: Rabbit anti-RAB5 (ABCam (ab218624), Cambridge, UK), Rabbit anti-RAB7 (ABCam (ab137029), Cambridge, UK), Rabbit anti-LAMP1 (Sigma (L1418), Saint Louis, MO) and incubated for 30 min. AlexaFluor 488 Goat anti-rabbit IgG (Invitrogen (A11034)) secondary antibody (Thermo Scientific, Waltham, MA, USA) was diluted into PBS-GSA solution containing 1% BSA and incubated for 30 min in the dark. Next, cells were washed twice with PBS-GSA and incubated for 5 min in the same solution. The antibody labelled cells were then mounted onto a slide using Prolong antifade Diamond mountant with DAPI (Thermo Scientific, Waltham, MA). After curing at room temperature, protected from the light, for 24 h the slides were visualized in Zeiss LSM800 confocal microscope (Carl Zeiss, Berlin, Germany) at the University of Florida ICBR Electron Microscopy Core Facility, RRID:SCR_019146. Colocalization was determined using the Zen Blue image analysis software. For this, the individual channels for the AlexaFlour 488 and AlexaFlour 594/rhodamine B were used to set the threshold on the image intensity scatterplot creating 4 quadrants. In this plot quadrant 3 indicated the colocalized pixels. The colocalization coefficient was calculated by summing the pixels in the colocalized region (Quadrant 3) and then dividing by the sum of pixels in Channel 1 (Quadrant 1 + Quadrant 3) or in Channel 2 (Quadrant 2 + Quadrant 3). Each pixel was assigned a value of 1. The colocalization coefficient values range from 0 to 1.

TABLE 1 Primers for qRT-PCR.

Primer name	Primer sequence (5′−3′)	Source
GAPDH Forward	GAAGGTGAAGGTCGGAGTC	(Teixeira et al., 2022)
GAPDH Reverse	GAAGATGGTGATGGGATT	(Teixeira et al., 2022)
OAS2 Forward	ACCCGAACAGTTCCCCCTGGT	*
OAS2 Reverse	ACAAGGGTACCATCGGAGTTGCC	*
MX2 Forward	CATGCATCAGGGGTCCACAC	*
MX2 Reverse	GGACTGGAGAGCCATCCCTT	*
IFI44L Forward	CAGCTTCCACGTGTGAGTGAG	*
IFI44L Reverse	ACGGCTGCATCTTTCAACCA	*

*Original to this work.

2.6 | mRNA extraction and qRT-PCR

RNA was extracted from eukaryotic cell lines using the Qiagen RNeasy Miniprep following manufacture's specifications (QIAGEN, Germantown, MD). Total RNA from *L. johnsonii* N6.2 bacterial cells or EV were extracted using Invitrogen RiboPure bacterial RNA extraction kit (Thermo Scientific, Waltham, MA). For the EV suspension in 1x PBS, a 1:10 ratio (V/V) of EV to Lysis/Binding Buffer (100 μL of vesicle suspension to 1 mL Lysis/Binding Buffer). The RNA extracted were assessed for concentration and purity using a NanoDrop One Microvolume UV–vis spectrophotometer (Thermo Scientific, Waltham, MA) and visually analyzed for degradation using a 1% agarose gel. qRT-PCR was performed using a QuantStudio 6 Flex (Thermo Scientific, Waltham, MA) as described (Teixeira et al., 2022). Primer sequences used to determine relative transcript abundance are listed in Table 1.

2.7 | Endosomal escape assay

βlox5 cells were grown in 6-well plates containing a poly-D-lysine-coated coverslip. Once cells reached confluence the media was removed and media containing 100 μg/mL of calcein was added in the absence or in the presence of EV or Alexa 594 labelled EV. The cells were incubated at 37°C for 0, 15, 30, 45, and 60 min. The cells were then fixed and prepared for immunofluorescence following the above-described protocol without the permeabilization step.

2.8 | EV treatment assays

For the RNase protection assay, the EV pellet was resuspended in 1 mL of PBS and treated with 0.5 μg/μL of RNase A (Thermo Scientific, Waltham, MA) for 20 min at 37°C to degrade extravesicular RNA. Next, the RNase-treated EV were recovered by ultracentrifugation as described above and resuspended in 500 μL of PBS or βlox5 media, as needed. EV disruption assays were performed by incubation of the concentrated EV at 100°C or 0.5% Triton X-100 for 10 min. The RNAse-treated or disrupted EV were then used to treat the βlox5 cell for qRT-PCR as described above.

2.9 | Bacterial lipid extraction and liposome formation

L. johnsonii N6.2 cultures were grown and harvested as described above. Cells were washed twice with 1% (w/v) NaCl then frozen at −80°C overnight and freeze-dried (Labconco, Kansas City, MO) for 24 h. Total lipids from *L. johnsonii* N6.2 were extracted using a modified Bligh and Dyer method (Lewis et al., 2000). In short, 1 g of freeze-dried cells was added into a clean glass separatory funnel and the following solvents were added, in sequence, to achieve a final chloroform:methanol:water ratio of 1:2:0.8 (v/v/v). The mixture was allowed to stand for 18 h with occasional shaking and subsequent phase separation was achieved by adding chloroform and water to reach a chloroform:methanol:water ratio of 1:1:0.9 (v/v/v). The lower chloroform phase was collected. Most of the solvent was evaporated in a rotavapor (Buchi, Switzerland) at 474 mbar and a water bath of 40°C. The remaining solvent was evaporated under a nitrogen stream and dried total lipid extractions were sealed in glass tubes and stored at −80°C until use. The dried total lipid extract was then resuspended in 1 mL of 1x PBS. The PBS lipid suspension is then extruded through a 0.1 μm polycarbonate membrane filter (Whatman-Cytiva, Marlborough, MA) an Avanti Mini-extruder following manufacturer's protocol (Avanti Polar Lipids, AL). For liposomes containing RNA, the quantified extruded liposomes were extruded again with the desired RNA amount.

2.10 | Bacterial or EV RNA transfection

Total RNA was extracted from *L. johnsonii* N6.2 or concentrated EV and quantified as described above. Next, 2.7 μg of the RNA was mixed with Lipofectamine LTX (Thermo Scientific, Waltham, MA) following manufacturers' protocol.

2.11 | RNA sequencing

Library construction and sequencing was performed by Novogene, (Novogene Co., Davis, CA) as follows. RNA purity was checked using the NanoPhotometer® spectrophotometer (IMPLEN, CA, USA), and RNA integrity and quantitation were assessed using the RNA Nano 6000 Assay Kit of the Bioanalyzer 2100 system (Agilent Technologies, CA, USA). A total amount of 1 μg RNA per sample was used as input material for the RNA sample preparations. Sequencing libraries were generated using NEBNext® UltraTM RNA Library Prep Kit for Illumina® (NEB, USA) following manufacturer's recommendations and index codes were added to attribute sequences to each sample. After cluster generation, the library preparations were sequenced on an Illumina platform and paired-end reads were generated. Raw data (raw reads) of FASTQ format were first processed through fastp. The reference genome (NCBI NC_022909.1) and gene model annotation files were downloaded from NCBI. Bowtie2 was used for both building index of reference genome and aligning clean reads to reference genome were used. FeatureCounts was used to count the read numbers mapped to each gene. FPKM, expected number of Fragments Per Kilobase of transcript sequence per Millions base pairs sequenced, of each gene was calculated based on the length of the gene and reads count mapped to the gene. Differential expression analysis between EV- and whole cell-derived RNA (three biological replicates each) was performed using the DESeq2 R package. The resulting p-values were adjusted using Benjamini and Hochberg's approach for controlling the false discovery rate. Genes with an adjusted p-value <0.05 and Log_2 fold change >1 or <−1 found by DESeq were assigned as differentially expressed. Gene Ontology (GO) enrichment analysis of differentially expressed genes was implemented by the clusterProfiler R package, in which gene length bias was corrected. GO terms with corrected p value less than 0.05 were considered significantly enriched by differential expressed genes. ClusterProfiler R package to test the statistical enrichment of differential expression genes in KEGG pathways. Post-sequencing quality control was done using RSeQC to measure the integrity of the transcripts. The Transcript Integrity Number (TIN) assigned ranges from 0 to 100 (Wang et al., 2016).

2.12 | Data and resource availability

The RNA sequencing data generated in this study are deposited in the NCBI Sequence Read Archive (SRA) under BioProject (PRJNA915103).

2.13 | Statistical analysis

GraphPad Prism 9.491 software (GraphPad Software, La Jolla, CA) and Origin 9.7.0.188 (OriginLab Corporation, Northampton, MA, USA) were used for data analysis and visualization. Statistical tests were performed using one-way analysis of variance (ANOVA) to evaluate the effects of treatments, followed by a Tukey posthoc test. Results were summarized as means ± standard deviation, and the significance of model terms and treatment comparisons were considered significant at a level of $\alpha = 0.05$, or otherwise specified. R studio (RStudio Team, Boston, MA) was used for data analysis and visualization of the RNAseq data.

3 | RESULTS

3.1 | βlox5 actively uptake *L. johnsonii* N6.2 EV

To evaluate the EV uptake mechanism, we compared the ζ potential between EV and the host cells. The ζ potential of *L. johnsonii* N6.2 EV and pancreatic βlox5 was determined by ZetaSizer Ultra (Malvern Instruments, Malvern, UK). The ζ potential of the *L. johnsonii* N6.2 EV was determined at −18.05 mV (±2.549 mV) while ζ potential of the βlox5 was measured at −26.84 mV (±1.603 mV). These results suggests that an active mechanism of uptake would be required for incorporation of the bacterial EV into the host cells.

Next, we determined if the cellular internalization of the EV are mediated by a passive or active mechanism. The βlox5 cells were incubated with AlexaFluor 594 labelled-EV, at 4°C and 37°C. The results obtained at specific time points (0, 15, 30 and 45 min) are depicted in Figure 1. It was found that after 15 min at 37°C the βlox5 cells showed accumulation of the EV mostly on the

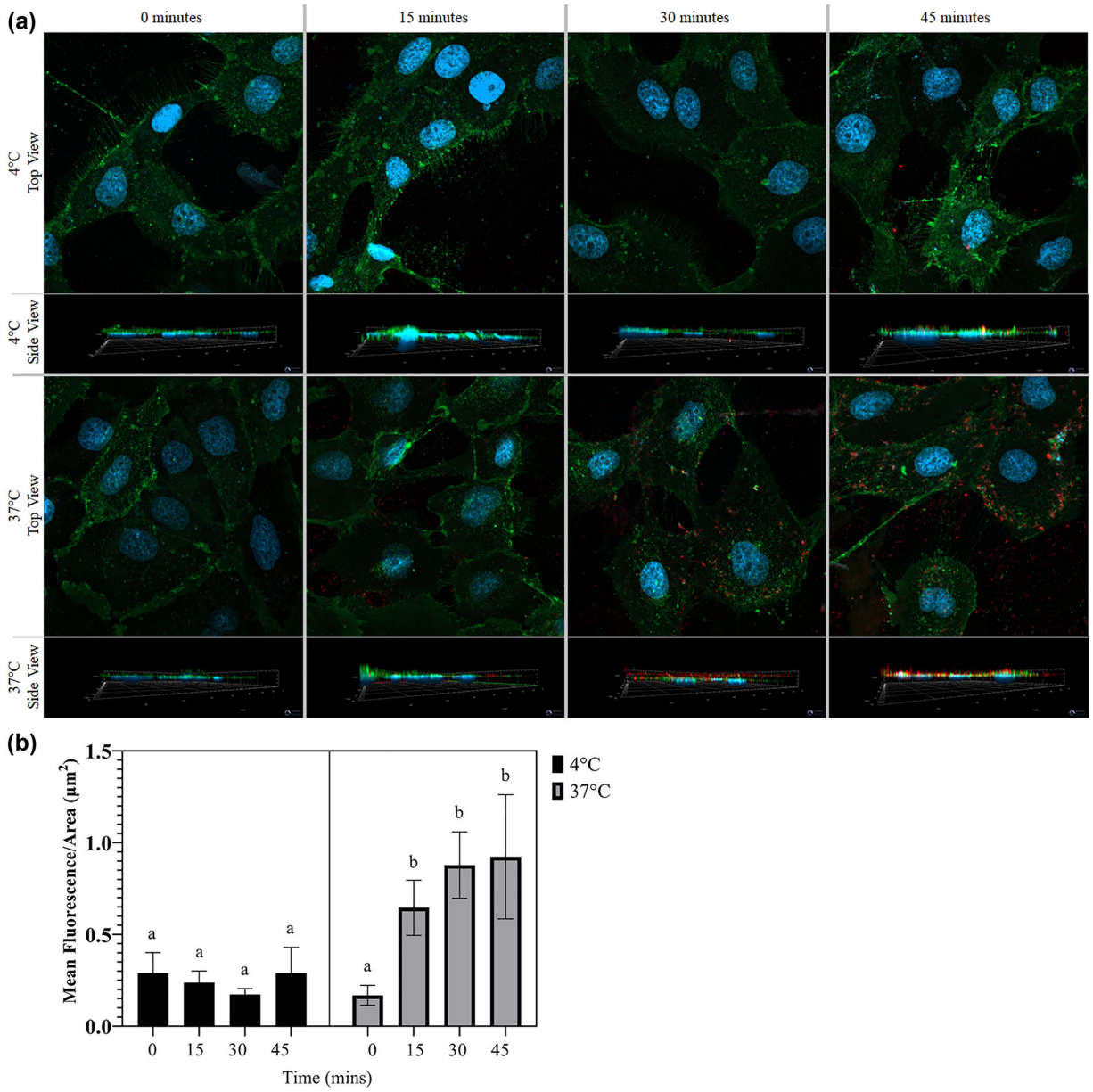

FIGURE 1 βLox5 cells in an energy depleted state (4°C) shows impairment in the internalization of *L. johnsonii* N6.2 labelled EV compared to βLox5 cells standard energy state (37°C). (a) βLox5 cells were treated with AlexaFluor 594 labelled EV for 0, 15, 30 and 45 min and incubated at 37°C or 4°C, as indicated on the side of each panel, and visualized by fluorescent confocal microscopy. Cell nucleus was stained with DAPI in cyan, the cell membrane was stained with AlexaFluor 488 WGA in green and the EV were stained with AlexaFluor 594 in red. Z-stacks were made with a composite of 15 images. (b) Quantification of the AlexaFluor 594 labelled EV signal per cell area, different letters on top of the corresponding bar indicated statistical significance of $p \leq 0.05$ from ANOVA analysis and post-hoc Tukey test performed on 10 individual cells.

cell surface. After 45 min of incubation at 37°C the signal was found in the cytoplasm with an almost uniform distribution. In contrast, cells incubated at 4°C did not show accumulation of EV after 15 min while significantly less accumulation was observed after 45 min when compared to the same time point in cells incubated at 37°C. These results indicate that EV are internalized by the βlox5 cells utilizing an energy-dependent active mechanism.

3.2 | EV are internalized by a clathrin/dynamin-dependent endocytosis

There are many energy-dependent mechanisms of internalization that cells can use to internalize the EV such as clathrin and caveolin mediated endocytosis, macropinocytosis and phagocytosis (Mulcahy et al., 2014). To evaluate which of these mechanisms are used to internalize *L. johnsonii* N6.2 EV, chlorpromazine (clathrin inhibitor), dynasore (dynamin inhibitor),

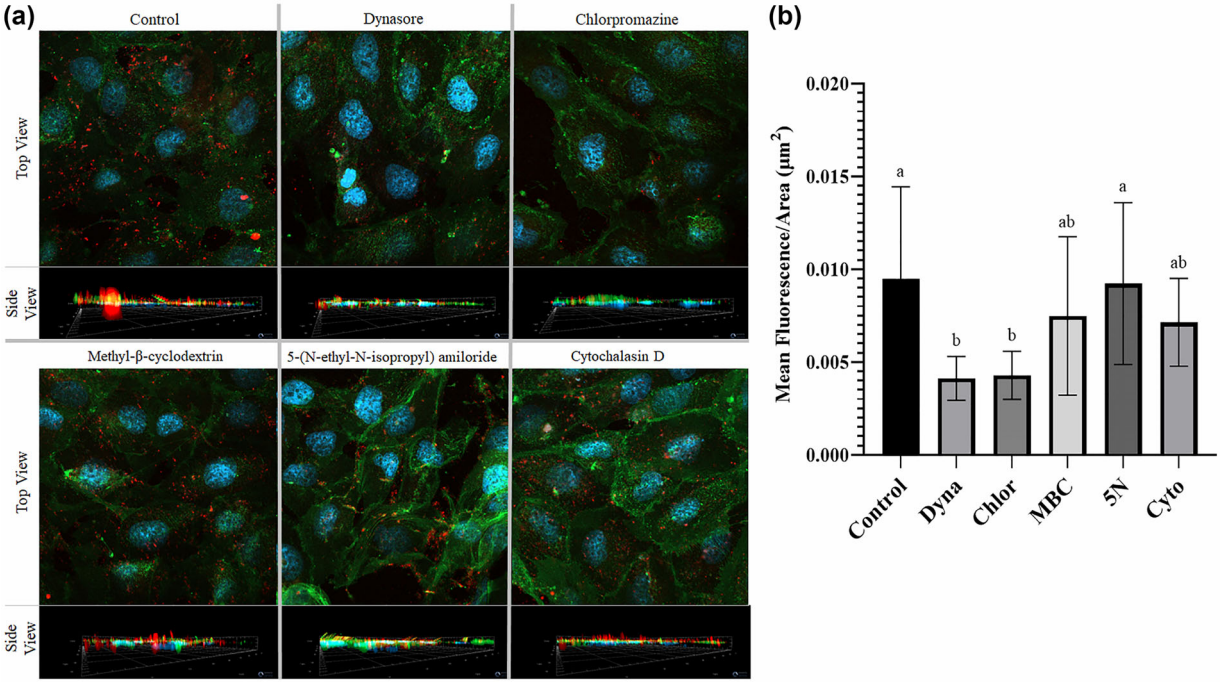

FIGURE 2 *L. johnsonii* N6.2 EV are internalized by a clathrin/dynamin dependent endocytic pathway. βLox5 cells were pretreated with 1.61 μL/mL of DMSO (Control), 80 μM of dynasore (Dyna), 0.5 μM of chlorpromazine (Chlor), 50 μM of methyl-β-cyclodextrin (MBC), 4 nM of 5(*N*-ethyl-*N*-isopropyl)-amiloride (5N) or 1 nM of cytochalasin D (Cyto), incubated with AlexaFluor 594 labelled EV and incubated at 37°C for 45 min, and visualized by fluorescent confocal microscopy. (a) Cell nucleus was stained with DAPI in cyan, the cell membrane was stained with AlexaFluor 488 WGA in green and the EV were stained with AlexaFluor 594 in red. Z-stacks were made with a composite of 15 images. (b) Quantification of the AlexaFluor 594 labelled EV signal per cell area, different letters on top of the corresponding bar indicated statistical significance of $p \leq 0.05$ from ANOVA analysis and post-hoc Tukey test performed on 10 individual cells.

methyl-β-cyclodextrin (lipid sequester), cytochalasin D (actin inhibitor) and 5(*N*-ethyl-*N*-isopropyl)-amiloride (macropinocytosis inhibitor) were used. The addition of both chlorpromazine and dynasore decreased the uptake and accumulation of EV evidenced by significant reduction of the Alexa 594 EV signal (Figure 2a). No significant differences were observed when testing the other inhibitors (Figure 2b). These results indicate that EV are internalized by the cell in a clathrin/dynamin-dependent mechanism. These results were validated by following the expression of host genes previously shown to be induced by *L. johnsonii* EV (Figure 3).

As reported earlier, βlox5 cells treated with the EV activates the expression of genes encoding for intracellular RNA sensing proteins such as *OAS1*, *OAS2*, *OASL*, *MX2*, *IFI44* and *IFI44L* (Teixeira et al., 2022). A time point experiment was performed to evaluate the kinetics of induction in expression of these genes in the presence of EV. It was found that while all genes tested in βlox5 cells were induced in the presence of EV, they reached the maximal induction level after 5 h (Figure S2). Since *OAS2*, *MX2* and *IFI44L* showed the greatest transcriptional change, these genes were chosen as markers of EV stimulations in the following experiments. Following a similar protocol as stated above, the effect of uptake inhibitors was tested on βlox5 cells in presence of EV for 1 h (the same time used for the visualization) and 5 h. While no differences in gene expression were observed after 1 h of treatment with EV or inhibitors, after 5 h it was found that cells pretreated with dynasore significantly decreased the EV stimulation of the expression of *OAS2, MX2* and *IFI44L* (Figure 3). However, the same inhibition is not observed with chlorpromazine. The apparent discrepancy may be explained by the longer incubation time needed to achieve peak transcriptional change when compared to the initial uptake experiments using labelled EV (Figure 2). The difference in incubation time would allow the cells to overcome the chlorpromazine mediated clathrin inhibition. Altogether, these results indicate that EV from *L. johnsonii* N6.2 are actively internalized by βlox5 cells by a dynamin-dependent endocytosis mechanism.

Next it was evaluated if the induction of the host RNA sensing genes may be triggered within the host endosome. While the endosome nucleic acid sensors TLR7 and TLR9 are not expressed in this cell line, the OAS1 variant p46 has been shown to colocalize with the endosomes in some cell lines (Teixeira et al., 2022; Wickenhagen et al., 2021). We evaluated whether the OAS1 p46 variant protein is expressed in βlox5 cells using Western blot analyses. It was found that βlox5 cells expressed the endosome associated p46 variant OAS1 protein, as well as the cytosol located p42 variant (Figure S3) (Lin et al., 2009; Marie et al., 1990; Rebouillat et al., 1999). These results suggest that the expression of this endosome associated OAS1 variant would allow for the early sensing of the EV RNA cargo within the endosome.

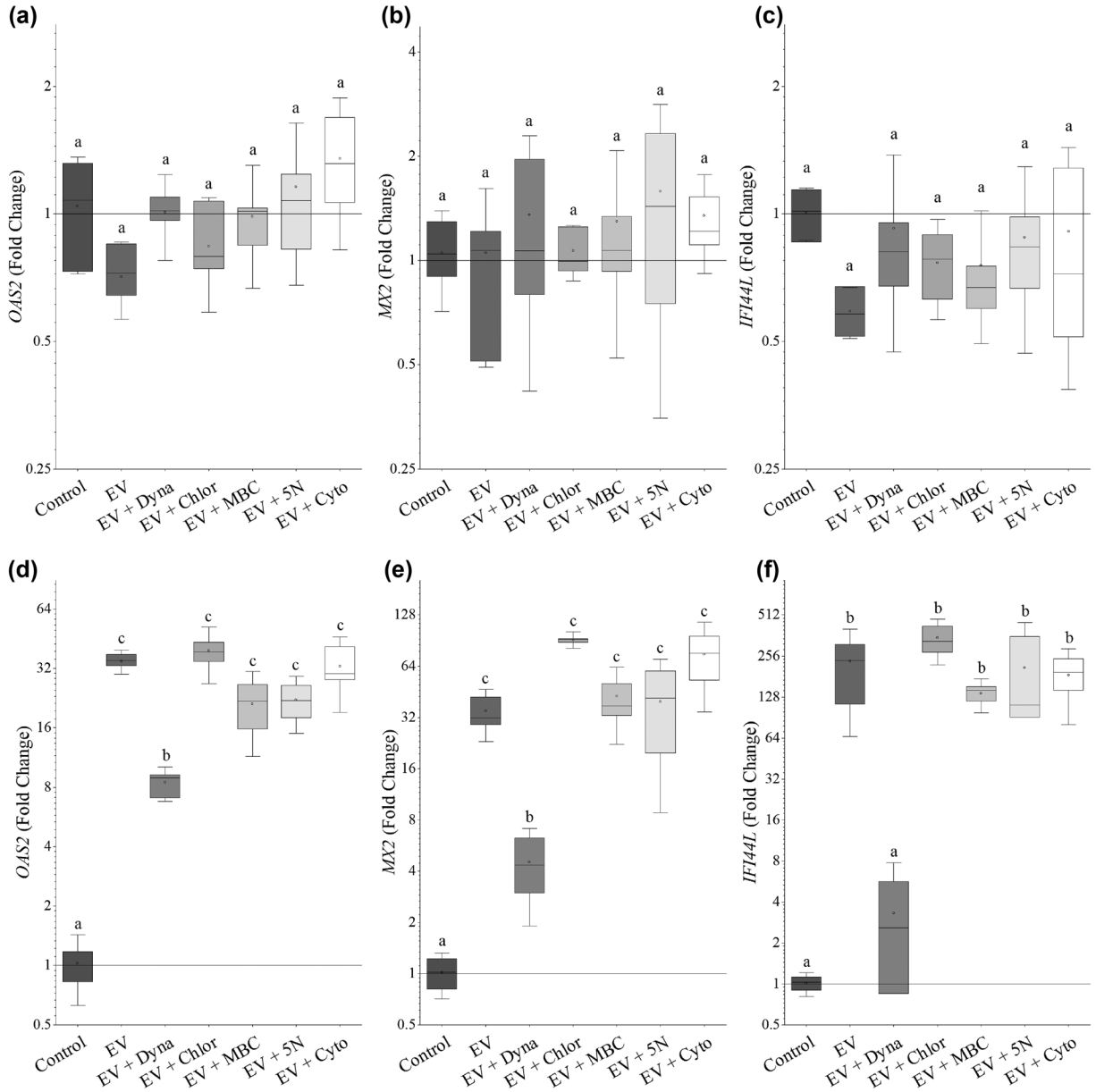

FIGURE 3 Inhibition of clathrin endocytic pathway hinders induction of the host RNA sensing genes. Cells were treated with *L. johnsonii* N6.2 EV and incubated at 37°C for 1 (a–c) or 5 h (d–f). βLox5 EV interaction was quantified using qRT-PCR and relative expression is shown as fold change for (a, d). *OAS2*, (b, e) *MX2* and (c, f) *IFI44L* when cells are pretreated with 1.61 μL/mL of DMSO (Control), 80 μM of dynasore (Dyna), 0.5 μM of chlorpromazine (Chlor), 50 μM of methyl-β-cyclodextrin (MBC), 4 nM of 5(*N*-ethyl-*N*-isopropyl)-amiloride (5N) or 1 nM of cytochalasin D (Cyto). Different letters on top of each bar indicates statistical significance of $p \leq 0.001$ from ANOVA analysis and post-hoc Tukey test performed on three biological replicates (with two qRT-PCR technical replicates each).

3.3 | EV are able to escape the endosome

To track the EV intracellular movement through the endosomal maturation process from early, late, and eventual lysosome fusion, antibodies specific to the RAB5, RAB7 and LAMP1 proteins, respectively, were used for immunofluorescence. Initial confocal microscopy analysis of βlox5 cells treated with the fluorescently labelled EV incubated at 37°C showed co-localization only at T0 with the RAB7 antibodies. These results suggested a quick uptake and processing of EV with transient early colocalization the late RAB7 markers, but not with the early marker RAB5 or the lysosome maker, LAMP1 (Figure S4). In order to observe the transient colocalization of the labelled EV and the endosomal markers, βlox5 cells were treated with prewarmed media containing the labelled EV and incubated at 4°C to slow the cellular endosomal processing. Confocal microscopy analysis of the cells showed that colocalization of the EV signal was observed with RAB5 early on and up to 7.5 min and colocalization with RAB7 after 10 min (Figure 4). These findings suggest that once the EV are internalized by the cell, they mature with the endosome, but

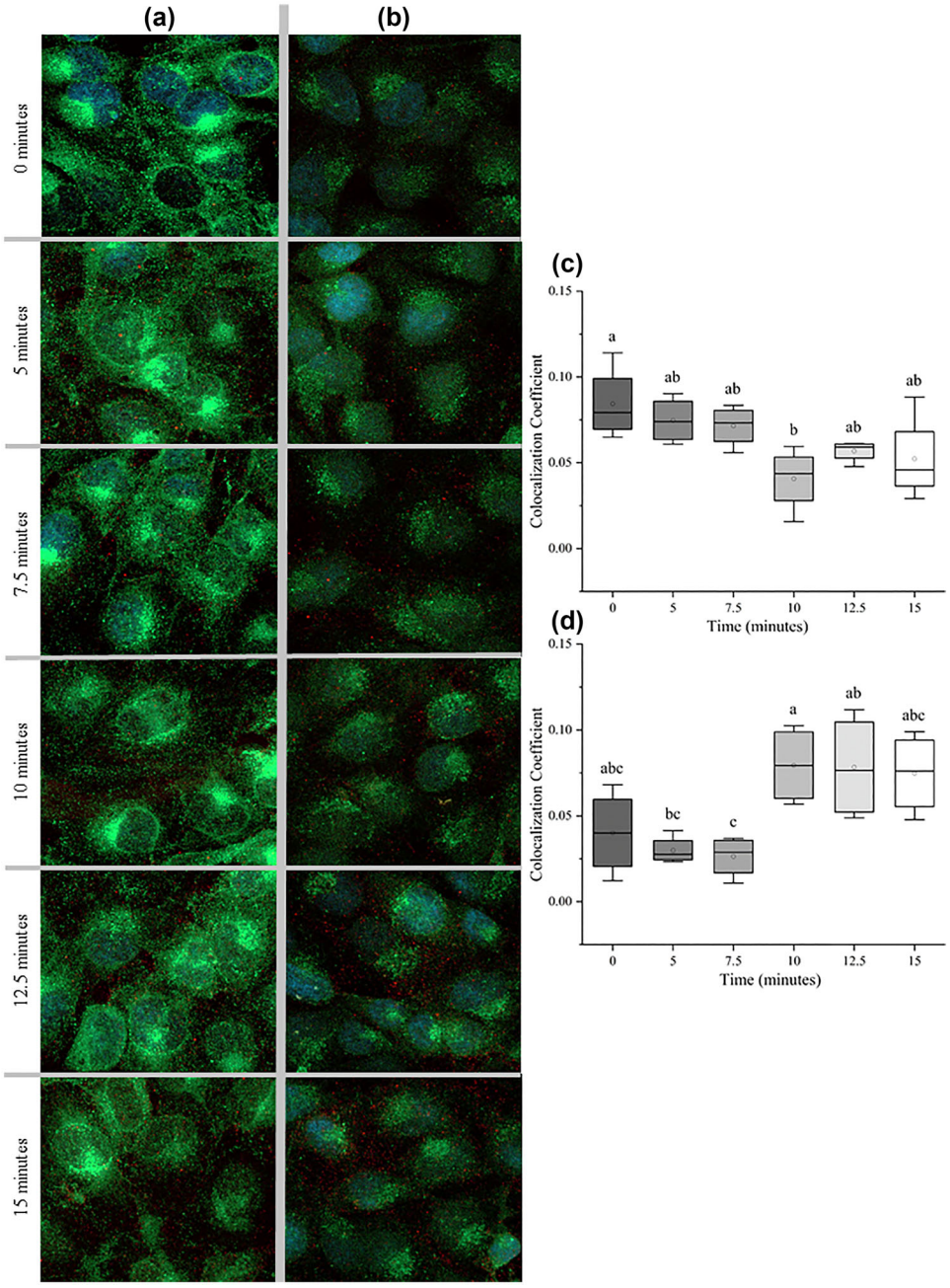

FIGURE 4 Colocalization of fluorescently labelled *L. johnsonii* N6.2 EV and early, late endosomal markers. Representative colocalization immunofluorescent images of (a) RAB5 and (b) RAB7 as shown in green and AlexaFluor 594 labelled EV in red. Colocalization coefficients of the EV and (c) RAB5 or (d) RAB7 signal. Different letters on top of the corresponding bar indicates statistical significance of $p \leq 0.05$ from ANOVA analysis and post-hoc Tukey test performed on 5 individual images.

they do not reach the lysosome stage. These results indicate a potential mechanism of endosomal escape by the EV by which the EV cargo may be delivered to the intracellular space. These results agree with the ability of *L. johnsonii's* EV to induce the expression of the *OAS1/2* genes which have previously been determined to have variants with cytoplasmic localization (Lin et al., 2009; Skrivergaard et al., 2019).

Next, we evaluated whether EV may escape early endosomes by following calcein distribution in βlox5 cells over time. Calcein is a cell impermeable fluorescent dye, which after uptake by the host cells accumulates within the endosome and lysosome and shows a punctuated phenotype as it cannot escape the intracellular endosomal membrane. Conversely, the addition of EV resulted in the diffusion of the dye into the cytoplasm over time, indicative of the escape of endosomal content. When rhodamine B labelled EV were used, it was observed that the EV and calcein were colocalized, however a decrease in the calcein diffusion phenotype was observed. We hypothesized the rhodamine B staining may affect the ability of EV to be released from the

endosome (Figure 5). These results suggest that upon incorporation of the EV, the endosome structure may be modified allowing their content to be released into the cytoplasm.

3.4 | EV structure is critical for RNA delivery

First, the role of the RNA component in the EV as the trigger of the cellular response was evaluated. To this end, total RNA extracted from *L. johnsonii* N6.2 cells or EV were transfected into βlox5 cells utilizing lipofectamine as the vehicle (Figure 6a–c). The concentration of RNA (2.7 μg) was selected based on the concentration of RNA found in 1×10^{10} EV. The expression of *OAS2*, *MX2* and *IFI44L* was used as a reporter of RNA sensing. It was found that total RNA from *L. johnsonii* N6.2, as well as the EV RNA in combination with lipofectamine, elicited a significant increase in the expression of *OAS2*, *MX2* and *IFI44L* genes when compared to native EV. The larger effect observed when using lipofectamine for RNA deliver may be explained by its cationic nature compared to the net negative charge that EV have. These results suggest that the RNA cargo of EV is the effector molecule targeting the induction of the RNA sensing genes.

To evaluate if the lipid component on the membrane of the EV would be responsible for the signalling response, we reconstituted liposomes using total lipids extracted from *L. johnsonii* N6.2. The liposomes were extruded through a 0.1 μm filter to produce similar sized particles as the native EV. The addition of liposomes to βlox5 cells did not stimulate the expression of *OAS2*, *MX2* and *IFI44L* genes indicating that lipids alone are not responsible for the effects observed with native EV (Figure 6d–f). Further, extrusion of lipids in presence or absence of *L. johnsonii* N6.2′s total cellular RNA or EV's RNA did not result in significant differences (Figure 6d–f). These results suggest that liposomes alone are either not able to be internalized by the host cell or that bacterial RNA may not be efficiently loaded in the liposomes. Another possibility is that a protein component present on the surface of the EV is required for binding and uptake into the βlox5 cells.

Next, to determine whether intravesicular or extravesicular RNA is responsible for the induction of RNA sensing genes in βlox5 cells, an RNase protection assay was performed. To remove extravesicular RNA, an RNase treatment was added during the EV purification step prior to the final wash and quantification. It was found that the treatment of βlox5 cells with RNase-treated EV showed similar levels of induction of the *OAS2*, *MX2* and *IFI44L* genes as the untreated EV. (Figure 7a–c). These findings indicate that extravesicular RNA that may be found in the EV preparation is not responsible for the cellular response.

Lastly, EV disruption assays were performed to evaluate the role of other components of the EV in uptake and/or delivery of the RNA cargo. EV were disrupted by incubation at 100°C or 0.5% Triton X-100 for 10 min. It was found that the disruption of the vesicle structure by both treatments significantly decreased the expression of *OAS2*, *MX2* and *IFI44L* genes in βlox5 cells (Figure 7d–i). These results indicate that the integrity of the EV is crucial for the likely internalization and subsequent modulation of the target genes involved in RNA sensing.

3.5 | The EV RNA content is skewed towards size, localization and whole cell abundancy

Next, we evaluated whether the composition of the RNA cargo present in the EV is different than the total RNA from *L. johnsonii* N6.2 cells. The initial evaluation of the RNA profiles indicated that the banding pattern obtained was different (Figure S5). The total RNA from the bacterial cells contained prominent banding patterns associated with the 23S and 16S ribosomal RNA, while in total RNA extracted from the EV the pattern was skewed towards fragments below that of the 16S ribosomal RNA (~1.6 kb). Global transcriptomic sequencing was used to identify whether specific sequences were enriched in the different fractions. Given the difference in banding pattern observed, the transcripts obtained from the RNA sequencing were analyzed for transcript integrity using a post-sequencing quality control (Wang et al., 2016). It was found that the cellular samples had a median TIN of 95.3 ± 0.8 while the EV samples had a median TIN of 93.8 ± 1.2, however, these differences were not statistically significant. These results indicate that while the total RNA profiles were different it is not related to degradation and suggest that a size exclusion process may be involved (Wang et al., 2016). Principal Component analysis allowed the visualization of the clustering of the samples with 80% of the variance explained by the source of the samples (Figure 8a). It was found that the transcripts found in the EV correlated with genes having an average length of 844 bp, significantly smaller than the cellular transcripts with an average of 972 bp (Figure 8b). These results are in agreement with the size distribution initially observed in the RNA gels.

Differential enrichment analysis was performed in RNA composition between the cellular and EV groups. Of the 1738 gene found in the *L. johnsonii* N6.2 genome, 516 genes were differentially enriched between the groups (p adjust value <0.05, $\log_2$ fold change >1 or <−1) with 239 enriched in the EV samples (Figure 8c). Transcripts were classified according to GO and KEGG terms to evaluate final localization of the protein encoded by the enriched transcripts as well as the pathways involved. Analysis of the enriched transcripts showed that the EV fraction contained significantly more transcripts for proteins with membrane or extracellular localization (Figure 8d).

Next, we investigated if overall transcript abundance is a predictor of transcript enrichment in the EV. Analysis of the KEGG pathways shows that ribosome and protein synthesis genes are the main pathway significantly enriched in the EV (Figure 8e).

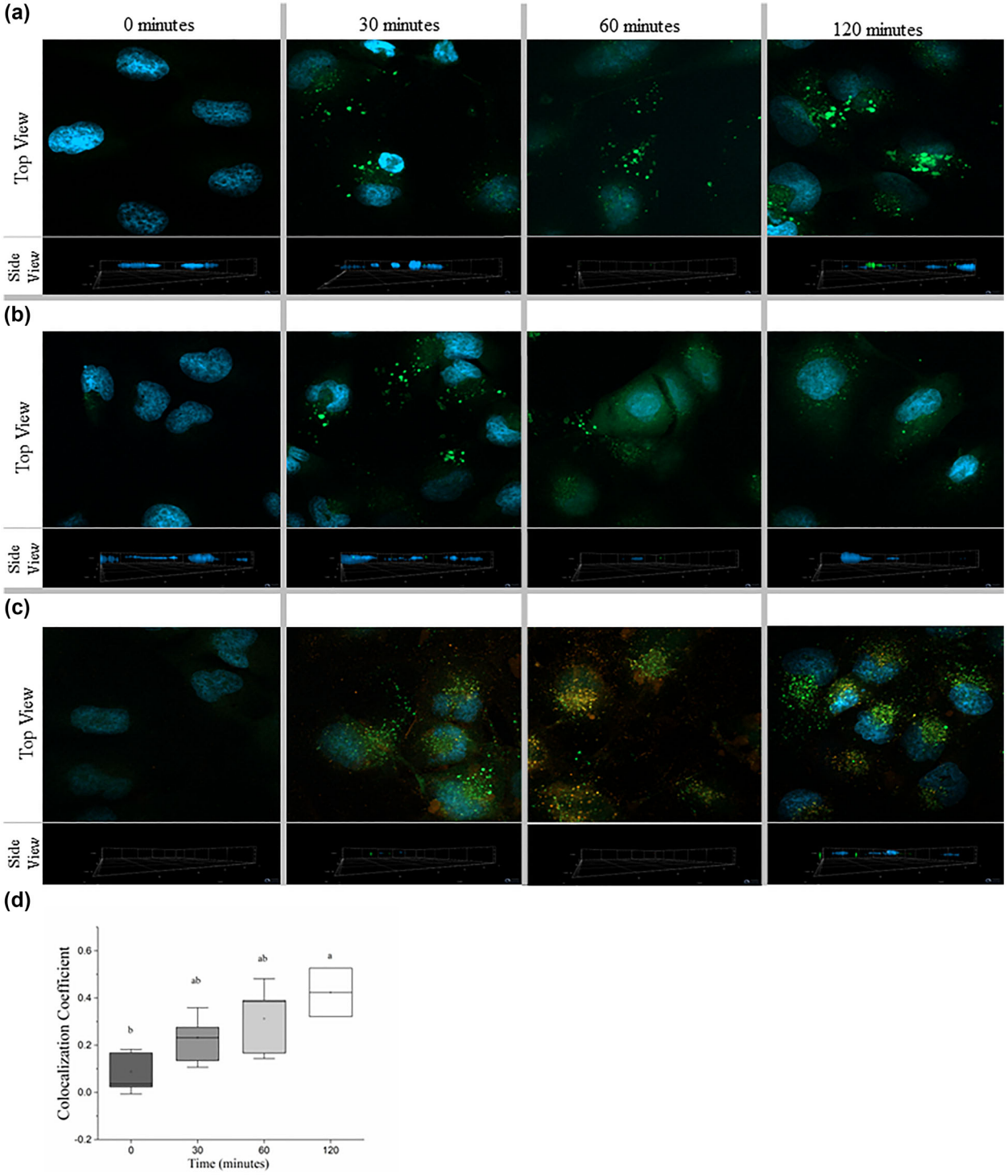

FIGURE 5 *L. johnsonii* N6.2 EV escape the late endosome. Representative images of the timepoint analysis of βLox5 incubated with media containing 100 μg/mL of calcein in the (a) absence and (b) presence of native *L. johnsonii* N6.2 EV or (c) Rhodamine B-labelled *L. johnsonii* N6.2 EV visualized by fluorescent confocal microscopy. Endosomal escape is evidenced by a cellular distribution of the calcein dye in green while endosomal retention shows a punctuated green phenotype. (d) Colocalization coefficient of the EV and calcein, different letters on top of the corresponding bar indicated statistical significance of $p \leq 0.05$ from ANOVA analysis and post-hoc Tukey test performed on 5 individual images.

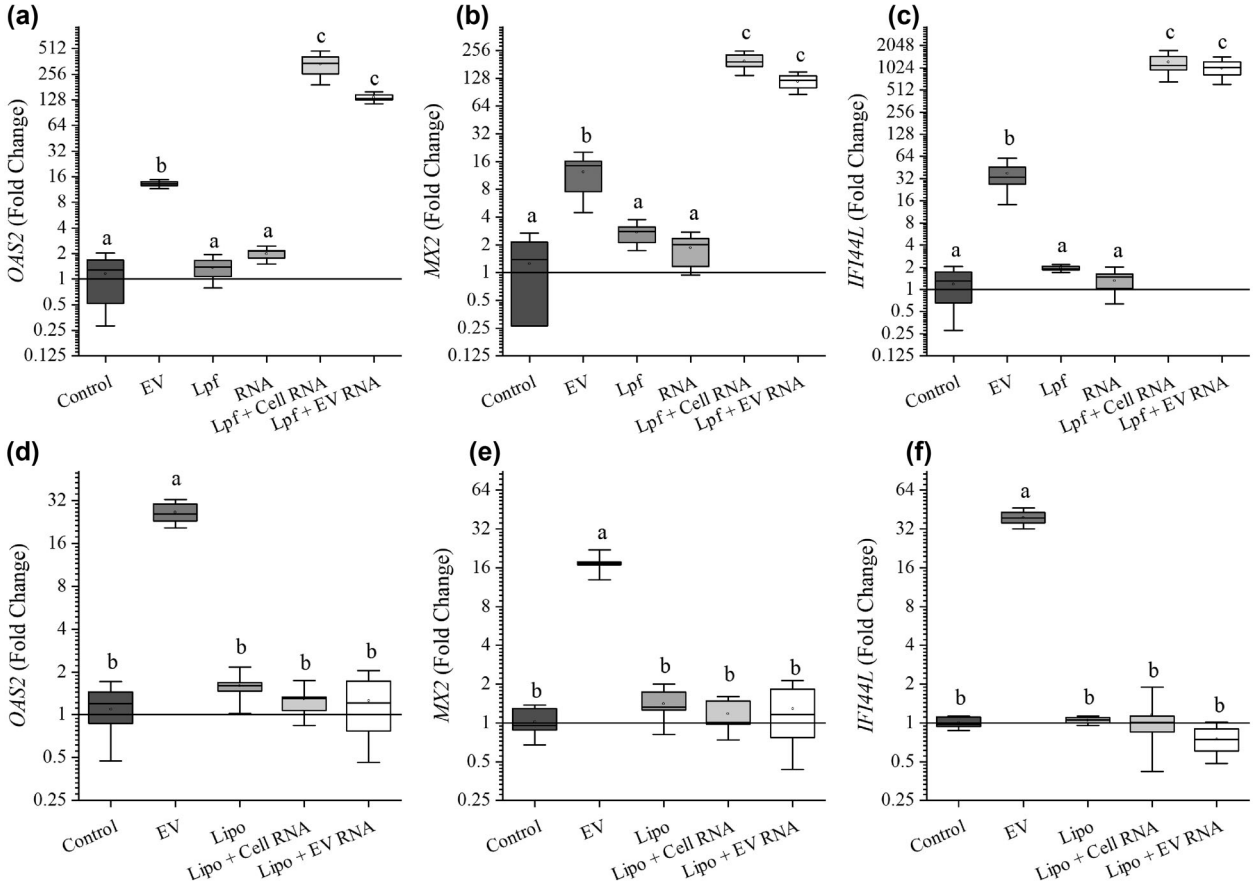

FIGURE 6 *L. johnsonii* N6.2 EV require a protein component to initiate cellular internalization while internalized RNA alone is sufficient to trigger a host RNA sensing response. (a–c) βLox5 cells treated with lipofectamine alone (Lpf), RNA alone and Lpf containing *L. johnsonii* N6.2 cellular RNA (Lpf + Cell RNA) or EV RNA (Lpf + EV RNA). (d–f) βLox5 cells were treated with protein-free liposomes (Lipo) made from total lipid extract from *L. johnsonii* N6.2 and Lipo containing cellular RNA (Lipo + Cell RNA) or EV RNA (Lipo + EV RNA). Relative gene expression shown as fold change for (a, d) *OAS2*, (b, e) *MX2* and (c, f) *IFI44L*. Different letters on top of each bar indicates statistical significance of $p \leq 0.001$ from ANOVA analysis and post-hoc Tukey test performed on three biological replicates (with two qRT-PCR technical replicates each).

Of the 239 EV enriched transcripts, 77 are associated with ribosome assembly and protein synthesis (54 ribosomal proteins, 8 translation factors, 12 tRNA modification genes and 3 chaperone genes) accounting for 32.2% of the EV enriched transcripts (Table S1). These results further confirm that the proportion of the transcripts enriched in the EV are derived from the most abundantly expressed genes. In the whole cell fraction, the top 24 genes accounted for about 50% of the transcript counts. Of these 24 genes, 42% (10 genes) are genes associated with ribosome assembly and protein synthesis; 42% (10 genes) are related to glycolysis and ATP production, 8% (2 genes) are part of the nucleic acid maintenance and the remaining 8% (2 genes) are membrane associated genes. The analyzes of the 24 transcripts with the highest abundance in the EV showed that 16 overlap with the transcripts highest in abundance within the cellular fraction. The other eight genes include the two additional membrane protein encoding genes indicating that localization of translation may be a factor during the transcript capture during EV biogenesis.

In summary, the global RNA sequencing indicated that the RNA cargo in the EV is determined by the overall abundancy of the transcripts, the size of the transcript, as well as the final localization of protein encoded by those transcripts. However, further studies are needed to identify if there are bacterial transcripts with a specific effect on the host response.

4 | DISCUSSION

There is an urgent need for the identification of bacterial effector molecules as mediators of beneficial host:microbe interactions. Specifically, the understanding of how bacterial EV can elicit a host response can aid in pathogenesis mitigation or in the identification of mechanisms involved in beneficial and commensal bacteria interactions with the host. As a step in that direction, we have previously shown that extracellular vesicles released by *L. johnsonii* N6.2 induce a tolerogenic M2 phenotype in human macrophages, reduce cytokine-induced apoptosis in human beta cell lines and stimulate insulin secretion in human islets

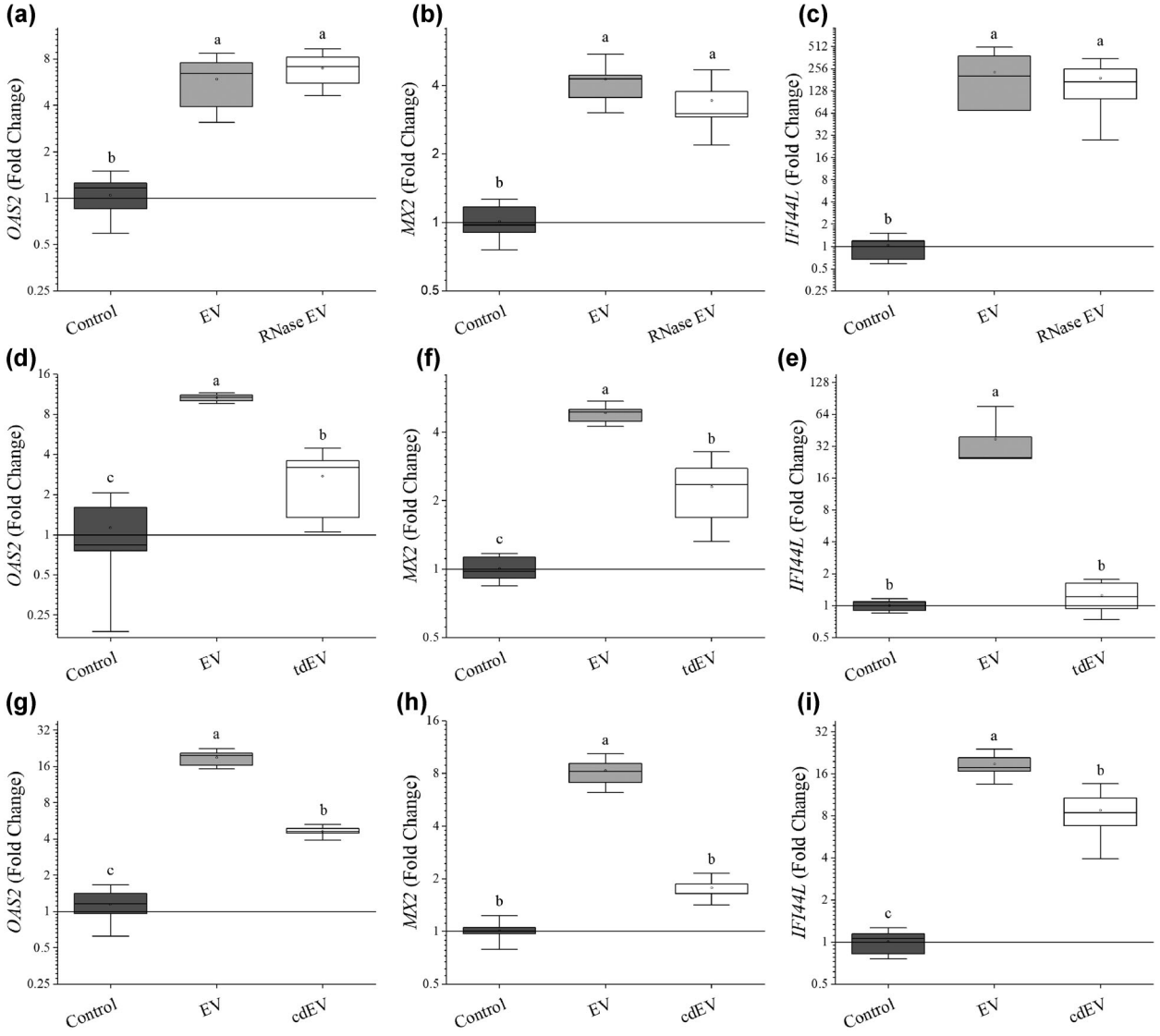

FIGURE 7 *L. johnsonii* N6.2 EV structure is critical in protecting the intravesicular cargo and in mediating the internalization into the host cell. (a–c) RNase protection assay was performed by treating EV with RNAse as described in the methods section. (d–i) EV were thermally disrupted (tdEV, d–f) by boiling for 10 min at 100°C or chemically disrupted (cdEV, g–i) by incubating the EV with 0.05% Triton X-100 for 10 min. βLox5 cells were incubated with the treated EV as indicated earlier. The impact of the treatments was followed by determining the relative expression of (a, d, g) *OAS2*, (b, e, h) *MX2* and (c, f, i) *IFI44L* genes. Different letters on top of each bar indicates statistical significance of $p \leq 0.001$ from ANOVA analysis and post-hoc Tukey test performed on three biological replicates (with two qRT-PCR technical replicates each).

(Teixeira et al., 2022). In this report, we determined the mechanism by which extracellular vesicles released by *L. johnsonii* N6.2 are internalized by human beta cell lines as well as key structural components involved in those interactions. Over the last few years, several reports have indicated that EV have an enriched cargo when compared to whole cells, however, information on critical macromolecules that act as mediators of uptake and transit is scarce.

There are many mechanisms by which eukaryotic cells can internalize extracellular content such as bacterial EV which may be dependent on their ζ potential. We found that *L. johnsonii* N6.2 EV ζ potential was in a similar negative range as the host βlox5 cells as well as to other human derived cell lines (in the range from −40.13 to −57.89 mV, Nishino et al., 2020). The net negative charge of the EV correlates with our lipidomic data which showed an enrichment of negatively charged polar phospholipids. The major contribution to the net charge is linked to the presence of cardiolipins, glycerophosphoglycerols and glycerophosphoethanolamines. These lipid species are 60% more abundant in the EV when compared to the amount observed in the cell membrane fraction (Harrison et al., 2021). These results indicated that the uptake of *L. johnsonii* N6.2 derived EV by the host cell is mediated by an active mechanism. This energy dependent mechanism would be required to overcome the repulsive forces caused by the similar negative potentials of the eukaryotic cell membrane and the EV.

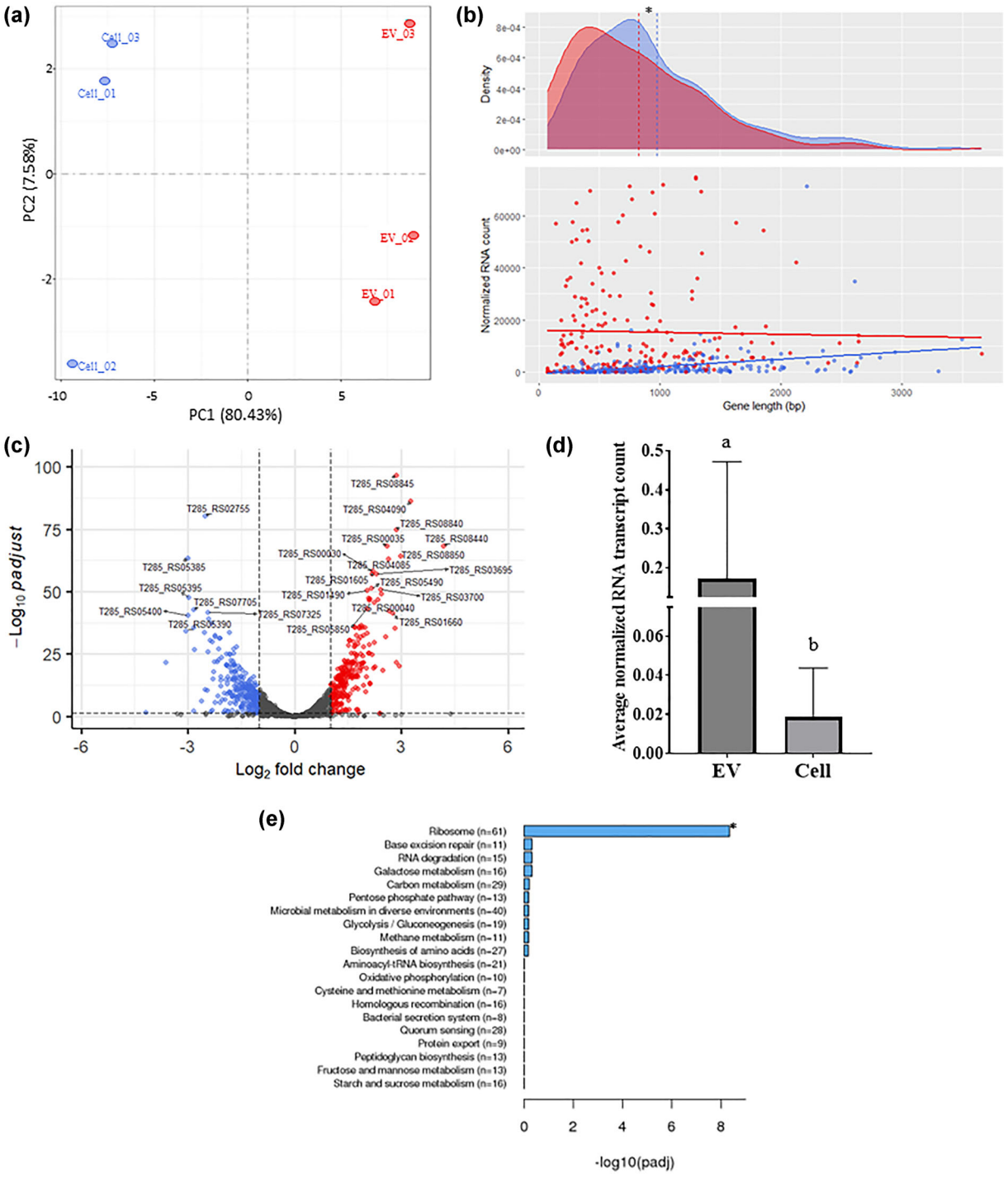

FIGURE 8 Global comparative transcriptomic analysis of the RNA in *L. johnsonii* N6.2 and its EV. (a) Principal component (PC) plot comparing the RNA content of the cellular and EV fractions, EV RNA samples are in red and cellular RNA samples are in blue. (b) Size analysis of the enriched transcripts within the cellular and EV fractions showing both the density distribution and count distribution according to gene length (dashed vertical lines represent average size). (c) Volcano plot of the differentially enriched transcripts within the cellular and EV fractions (red represents EV enrichment and blue represents cellular enrichment). (d) Comparison of the average normalized transcript count of the genes encoding for membrane and extracellular localized proteins. EV enriched RNA fraction (red) and the cellular enriched RNA fraction (blue). Different letters on top of each bar indicates statistical significance of $p \leq 0.05$ from student's *t*-test. (e) KEGG pathway analysis of the enriched transcript found within the EV compared against the cellular fraction (* indicates a statistical significance of $p \leq 0.05$).

Many studies have focused on the impacts of EV on phagocytic immune cells that readily internalize extracellular content. For nonphagocytic cells like βlox5, the literature so far has shown that bacterial EV use three mechanisms for cellular internalization, dynamin mediated endocytosis, clathrin mediated endocytosis and membrane fusion (Briaud & Carroll, 2020). Utilizing chemical inhibitors, we identified that *L. johnsonii* N6.2 EV are incorporated through the clathrin and dynamin pathway. Dynamin aids in the endosomal release from the membrane into the intracellular space from the membrane invagination caused from other process such as clathrin mediated endocytosis, explaining how two separate inhibitors can decrease cellular uptake of the vesicles. From the growing body of research on the topic of bacterial EV:host interaction, there is ample evidence that the internalization of EV is dependent on the species of the bacterial EV source as well as on the host cell type. For example, the OMVs produced by the enterotoxin producing *Escherichia coli* ATCC 43886 pathogenic strain have been shown to be internalized by a cholesterol-rich lipid raft endocytosis mechanism, while the probiotic *E. coli* Nissle 1917 strain was shown to be internalized by clathrin-dependent endocytosis in the human colorectal cell HT-29 (Cañas et al., 2016; Kesty et al., 2004). Another example is the EV from *S. aureus* ATCC 14458 were shown to be internalized by dynamin-dependent endocytosis with human macrophage cell THP-1, while *S. aureus* JE2 EV showed to be internalized by a cholesterol-rich lipid raft endocytosis mechanism in the same cell line (Gurung et al., 2011; Wang et al., 2020).

Once EV are internalized, most EV follow localization to a variety of compartments were it exerts its effects. Recently, OMVs from the Gram-negative *Legionella pneumophila* were shown to localize to the ER where its RNA cargo served as a potential source of interfering with RNA modulating cellular function (Sahr et al., 2022). Conversely, OMVs from the probiotic *E. coli* Nissle 1917 were shown to be sorted to lysosomal compartments for degradation (Cañas et al., 2016). However, the LPS composition of the OMVs allowed for cells to sense these OMVs and induce cellular changes. In this study, we were interested in elucidating the transit of EV following uptake as we previously shown that two clear pathways are transcriptionally induced when βlox5 are treated with the *L. johnsonii* N6.2 EV. Both of these pathways, the AHR pathway and the RNA sensing and degradation response, are of cytoplasmic localization. It was found that *L. johnsonii* N6.2 EV escape the endosome compartment shortly after uptake and induce a robust RNA sensing response. The endosomal escape of the *L. johnsonii* N6.2 EV is an interesting finding as it has not been studied within this genus so far. EV from *Bacillus subtillis* have been shown to transcytose polarized HT-29 cells, a mechanism in which many bacterial EV are theorized to do (Rubio et al., 2020). Transcytosis, similar to endosomal escape, evades lysosomal degradation of the internalized endosomal content and can explain how EV from bacterial sources found within the gastrointestinal system can have systemic effects. However, endosomal escape of a biologically active EV address one of the most difficult hurdles to overcome, the other being cellular tropism, in the development of biologics and intracellular delivery of its bioactive components. Although further research is needed to fully understand the host distribution of these EV, this is an essential step in elucidating these EV's mode of action.

Another understudied area of bacterial EV biogenesis is the understanding of the potential selectivity of the cargo loading. The RNA cargo of Gram-negative OMVs are limited to nucleic acids that can escape the cell and enter the periplasm to be incorporated into the OMVs, usually small RNA fragments (Sahr et al., 2022). Previous studies have shown the Gram-positive derived EV contain a more robust nucleic acid content compared to Gram-negative derived OMVs (Rodriguez & Kuehn, 2020). These findings may be explained by the biogenesis of Gram-positive bacteria EV from its cellular membrane, giving these EV access to cytoplasmic components including the whole cell transcriptome. In agreement with these observations are our findings that the most abundant transcripts found in the cell are also found within the EV in *L. johnsonii*. Nevertheless, transcript size also plays a key factor in the selectivity of the RNA EV cargo by a mechanism that is different than the OMV size selectivity. Given that the EV biogenesis originated on the cellular membrane, and that bacteria have coupled transcription/translation processes, it was hypothesized that transcripts for proteins which will be membrane bound or secreted would be preferentially found within the EV. Analysis of the enriched transcripts in whole cells compared to EV showed that the EV fraction contained statistically more transcripts for proteins of membrane or extracellular localization.

The intracellular distribution of the bacterial EV, once internalized in the host cell, can provide further insights into the mechanism of the EV:host interaction. We hypothesize that the initial internalization of bacterial EV into endosomes within the host cell may begin the sensory process by eliciting a response through endosome associated TLRs, such as TLR9 and TLR7 (if expressed by the target cell). This is in agreement with our previous reports where cell-free extract of the *L. johnsonii* N6.2 were shown to induce TLR9 and TLR7 expression in Caco2 cells (Kingma et al., 2011). Alternatively, the endosome associated p46 variant of the OAS1 protein may act as the initial response to the RNA cargo, as shown here (Kingma et al., 2011; Wickenhagen et al., 2021). An interesting finding downstream of endosome signalling, was that the genes induced by the *L. johnsonii* N6.2 EV are associated with exogenous RNA sensing and degradation (*OAS1, OAS2* and *OASL*), the induction of an antiviral cellular immune response (*MX1* and *MX2*) and immune modulation (*IFI44* and *IFI44L*). The induction of these antiviral genes has been shown to control viral infections aiding in both cellular and host survival to viral insults as they are critical in repressing the viral replication and initiating an innate immune response (Busse et al., 2020; Liu et al., 2013; Wickenhagen et al., 2021). This innate immune response may, depending on the context, lead to inflammatory response mediated by cytokines such as interferons and interleukins. For example, we observed the induction of *IFI44L* by cells treated with the *L. johnsonii* N6.2 EV even in the apparent absence of IFN stimulation. IFI44L has been proposed as a regulator of host antiviral response following a viral infection controlling deleterious excessive innate immune response (DeDiego et al., 2019). This finding is interesting in the context of a potential application to

mitigation of autoimmune T1D onset. The epidemiology of T1D is complex and not fully understood, however, a leaky gut and viral infection have been hypothesized as early triggers of T1D onset (Acharjee et al., 2013; Hamilton-Williams et al., 2021). We speculate that the strong induction of an antiviral response along with a strong immune regulation induced by the *L. johnsonii* N6.2 EV may be a mechanistic pathway by which *L. johnsonii* N6.2 may beneficially impact the host, potentially delaying or even preventing the onset of T1D.

Table S1. RNA transcripts enrichment in the EV and cellular fractions identified by global transcriptomics. Transcript enrichment is defined as a padjust ≤ 0.05 and log2 fold change ≥ 1 for the EV fraction and padjust ≤ 0.05 and log2 fold change ≤ −1 for the cellular fraction.

AUTHOR CONTRIBUTIONS

Danilo Rodrigues da Silva: Conceptualization; formal analysis; investigation; methodology; visualization; writing—original draft; writing—review & editing. **Claudio Fabricio Gonzalez**: Conceptualization; funding acquisition; investigation; methodology; supervision; writing—original draft; writing—review & editing. **Graciela Lorca**: Conceptualization; funding acquisition; investigation; methodology; project administration; resources; supervision; writing—original draft; writing—review & editing

ACKNOWLEDGMENTS

We acknowledge Dr. Peter Kima, Dr. Natalie Harrison, Dr. Leandro Teixeira, Alexandra Cuaycal, Alexandra Davis and Amanda Elias for their technical help and fruitful scientific discussions. We thank Reagan Beliakoff for the critical reading of the manuscript. This study was funded by the National Institute of Diabetes and Digestive and Kidney Diseases of the National Institutes of Health under award number R01DK121130. The content is solely the responsibility of the authors and does not necessarily represent the official views of the National Institutes of Health.

CONFLICT OF INTEREST STATEMENT

Dr. Graciela Lorca holds U.S. patent No. 9474773 and 9987313 on *Lactobacillus johnsonii* N6.2. The remaining authors declare that the research was conducted in the absence of any commercial or financial relationships that could be construed as a potential conflict of interest.

DATA AVAILABILITY STATEMENT

The datasets presented in this study can be found in the NCBI SRA online repository. The BioProject number is PRJNA915103.

ORCID

Graciela Lorca https://orcid.org/0000-0001-7525-7589

REFERENCES

Acharjee, S., Ghosh, B., Al-Dhubiab, B. E., & Nair, A. B. (2013). Understanding type 1 diabetes: Etiology and models. *Canadian Journal of Diabetes*, *37*(4), 269–276. https://doi.org/10.1016/j.jcjd.2013.05.001

Briaud, P., & Carroll, R. K. (2020). Extracellular vesicle biogenesis and functions in gram-positive bacteria. *Infection and Immunity*, 88(12). American Society for Microbiology. https://doi.org/10.1128/IAI.00433-20

Busse, D. C., Habgood-Coote, D., Clare, S., Brandt, C., Bassano, I., Kaforou, M., Herberg, J., Levin, M., Eléouët, J. F., Kellam, P., & Tregoning, J. S. (2020). Interferon-induced protein 44 and interferon-induced protein 44-like restrict replication of respiratory syncytial virus. *Journal of Virology*, *94*(18), 10–1128. https://doi.org/10.1128/jvi.00297-20

Cañas, M. A., Giménez, R., Fábrega, M. J., Toloza, L., Baldomà, L., & Badia, J. (2016). Outer membrane vesicles from the probiotic *Escherichia coli* Nissle 1917 and the commensal ECOR12 enter intestinal epithelial cells via clathrin-dependent endocytosis and elicit differential effects on DNA damage. *PLoS ONE*, *11*(8), e0160374. https://doi.org/10.1371/journal.pone.0160374

Chatterjee, D., & Chaudhuri, K. (2011). Association of cholera toxin with *Vibrio cholerae* outer membrane vesicles which are internalized by human intestinal epithelial cells. *FEBS Letters*, *585*(9), 1357–1362. https://doi.org/10.1016/j.febslet.2011.04.017

Chatterjee, S. N., & Das, J. (1967). Electron microscopic observations on the excretion of cell-wall material by Vibrio cholerae. *Microbiology*, *49*(1), 1–11.

Choi, E. J., Lee, H. G., Bae, I. H., Kim, W., Park, J., Lee, T. R., & Cho, E. G. (2018). *Propionibacterium acnes*-derived extracellular vesicles promote acne-like phenotypes in human epidermis. *Journal of Investigative Dermatology*, *138*(6), 1371–1379. https://doi.org/10.1016/j.jid.2018.01.007

Cossart, P., & Helenius, A. (2014). Endocytosis of viruses and bacteria. *Cold Spring Harbor Perspectives in Biology*, *6*(8), a016972. https://doi.org/10.1101/cshperspect.a016972

Dean, S. N., Rimmer, M. A., Turner, K. B., Phillips, D. A., Caruana, J. C., Hervey, W. J., Leary, D. H., & Walper, S. A. (2020). *Lactobacillus acidophilus* membrane vesicles as a vehicle of bacteriocin delivery. *Frontiers in Microbiology*, *11*, 710. https://doi.org/10.3389/fmicb.2020.00710

DeDiego, M. L., Martinez-Sobrido, L., & Topham, D. J. (2019). Novel Functions of IFI44L as a Feedback Regulator of Host Antiviral Responses. *Journal of Virology*, *93*(21), 10–1128. https://doi.org/10.1128/jvi.01159-19

Feng, D., Zhao, W. L., Ye, Y. Y., Bai, X. C., Liu, R. Q., Chang, L. F., Zhou, Q., & Sui, S. F. (2010). Cellular internalization of exosomes occurs through phagocytosis. *Traffic*, *11*(5), 675–687. https://doi.org/10.1111/j.1600-0854.2010.01041.x

Gandham, S., Su, X., Wood, J., Nocera, A. L., Alli, S. C., Milane, L., Zimmerman, A., Amiji, M., & Ivanov, A. R. (2020). Technologies and standardization in research on extracellular vesicles. *Trends in Biotechnology*, *38*(10), 1066–1098. Elsevier Ltd. https://doi.org/10.1016/j.tibtech.2020.05.012

Gurung, M., Moon, D. C., Choi, C. W., Lee, J. H., Bae, Y. C., Kim, J., Lee, Y. C., Seol, S. Y., Cho, D. T., Kim, S. I., & Lee, J. C. (2011). *Staphylococcus aureus* produces membrane-derived vesicles that induce host cell death. *PLoS ONE*, *6*(11), e27958. https://doi.org/10.1371/journal.pone.0027958

Halvorsen, T. L., Leibowitz, G., & Levine, F. (1999). Telomerase activity is sufficient to allow transformed cells to escape from crisis. *Molecular And Cellular Biology*, *19*(3), 1864–1870.

Hamilton-Williams, E. E., Lorca, G. L., Norris, J. M., & Dunne, J. L. (2021). A triple threat? The role of diet, nutrition, and the microbiota in T1D pathogenesis. *Frontiers in Nutrition*, 8, 600756. https://doi.org/10.3389/fnut.2021.600756

Harrison, N. A., Gardner, C. L., da Silva, D. R., Gonzalez, C. F., & Lorca, G. L. (2021). Identification of Biomarkers for Systemic Distribution of Nanovesicles From Lactobacillus johnsonii N6.2. *Frontiers in Immunology*, *12*, 723433. https://doi.org/10.3389/fimmu.2021.723433

Hong, S. W., Kim, M. R., Lee, E. Y., Kim, J. H., Kim, Y. S., Jeon, S. G., Yang, J. M., Lee, B. J., Pyun, B. Y., Gho, Y. S., & Kim, Y. K. (2011). Extracellular vesicles derived from *Staphylococcus aureus* induce atopic dermatitis-like skin inflammation. *Allergy: European Journal of Allergy and Clinical Immunology*, *66*(3), 351–359. https://doi.org/10.1111/j.1398-9995.2010.02483.x

Kesty, N. C., Mason, K. M., Reedy, M., Miller, S. E., & Kuehn, M. J. (2004). Enterotoxigenic *Escherichia coli* vesicles target toxin delivery into mammalian cells. *EMBO Journal*, *23*(23), 4538–4549. https://doi.org/10.1038/sj.emboj.7600471

Kingma, S. D. K., Li, N., Sun, F., Valladares, R. B., Neu, J., & Lorca, G. L. (2011). *Lactobacillus johnsonii* N6.2 stimulates the innate immune response through toll-like receptor 9 in Caco-2 cells and increases intestinal crypt Paneth cell number in BioBreeding diabetes-prone rats. *Journal of Nutrition*, *141*(6), 1023–1028. https://doi.org/10.3945/jn.110.135517

Lewis, T., Nichols, P. D., & Mcmeekin, T. A. (2000). Evaluation of extraction methods for recovery of fatty acids from lipid-producing microheterotrophs. *Journal of Methods Microbiological Journal of Microbiological Methods*, *43*, 107–116. https://www.elsevier.com/locate/jmicmeth

Lin, R. J., Yu, H. P., Chang, B. L., Tang, W. C., Liao, C. L., & Lin, Y. L. (2009). Distinct antiviral roles for human 2′,5′-oligoadenylate synthetase family members against dengue virus infection. *The Journal of Immunology*, *183*(12), 8035–8043. https://doi.org/10.4049/jimmunol.0902728

Liu, Z., Pan, Q., Ding, S., Qian, J., Xu, F., Zhou, J., Cen, S., Guo, F., & Liang, C. (2013). The interferon-inducible MxB protein inhibits HIV-1 infection. *Cell Host and Microbe*, *14*(4), 398–410. https://doi.org/10.1016/j.chom.2013.08.015

Marie, I., Svab, J., Robert, N., Galabru, J., & Hovanessian, A. G. (1990). Differential expression and distinct structure of 69- and 100-kDa forms of 2–5A synthetase in human cells treated with interferon. *Journal of Biological Chemistry*, *265*(30), 18601–18607. https://doi.org/10.1016/s0021-9258(17)44794-6

Mathieu, M., Martin-Jaular, L., Lavieu, G., & Théry, C. (2019). Specificities of secretion and uptake of exosomes and other extracellular vesicles for cell-to-cell communication. *Nature Cell Biology*, *21*(1), 9–17. Nature Publishing Group. https://doi.org/10.1038/s41556-018-0250-9

Mulcahy, L. A., Pink, R. C., & Carter, D. R. F. (2014). Routes and mechanisms of extracellular vesicle uptake. *Journal of Extracellular Vesicles*, 3(1), 24641. Co-Action Publishing. https://doi.org/10.3402/jev.v3.24641

Nano, P. R., Johnson, T. K., Kudo, T., Mooney, N. A., Ni, J., Demeter, J., Jackson, P. K., & Chen, J. K. (2021). Structure-activity mapping of ARHGAP36 reveals regulatory roles for its GAP homology and C-terminal domains. *PloS One*, *16*(5), e0251684.

Nishino, M., Matsuzaki, I., Musangil, F. Y., Takahashi, Y., Iwahashi, Y., Warigaya, K., Kinoshita, Y., Kojima, F., & Murata, S. (2020). Measurement and visualization of cell membrane surface charge in fixed cultured cells related with cell morphology. *PLoS ONE*, *15*(7), e0236373. https://doi.org/10.1371/journal.pone.0236373

Pan, B. T., Teng, K., Wu, C., Adam, M., & Johnstone, R. M. (1985). Electron microscopic evidence for externalization of the transferrin receptor in vesicular form in sheep reticulocytes. *The Journal of Cell Biology*, *101*(3), 942–948.

Rebouillat, D., Hovnanian, A., Marié, I., & Hovanessian, A. G. (1999). The 100-kDa 2′,5′-oligoadenylate synthetase catalyzing preferentially the synthesis of dimeric pppA2′p5′A molecules is composed of three homologous domains. *Journal of Biological Chemistry*, *274*(3), 1557–1565.

Rivera, J., Cordero, R. J. B., Nakouzi, A. S., Frases, S., Nicola, A., & Casadevall, A. (2010). *Bacillus anthracis* produces membrane-derived vesicles containing biologically active toxins. *Proceedings of the National Academy of Sciences of the United States of America*, *107*(44), 19002–19007. https://doi.org/10.1073/pnas.1008843107

Rodriguez, B. v., & Kuehn, M. J. (2020). *Staphylococcus aureus* secretes immunomodulatory RNA and DNA via membrane vesicles. *Scientific Reports*, *10*(1), 18293. https://doi.org/10.1038/s41598-020-75108-3

Rubio, A. P. D., Martínez, J., Palavecino, M., Fuentes, F., López, C. M. S., Marcilla, A., Pérez, O. E., & Piuri, M. (2020). Transcytosis of *Bacillus subtilis* extracellular vesicles through an in vitro intestinal epithelial cell model. *Scientific Reports*, *10*(1), 3120. https://doi.org/10.1038/s41598-020-60077-4

Sahr, T., Escoll, P., Rusniok, C., Bui, S., Pehau-Arnaudet, G., Lavieu, G., & Buchrieser, C. (2022). Translocated *Legionella pneumophila* small RNAs mimic eukaryotic microRNAs targeting the host immune response. *Nature Communications*, *13*(1), 762. https://doi.org/10.1038/s41467-022-28454-x

Schrier, S. L., Godin, D., Gould, R. G., Swyryd, B., Junga, I., & Seeger, M. (1971). Characterization of microvesicles produced by shearing of human erythrocyte membranes. *Biochimica et Biophysica Acta (BBA)-Biomembranes*, *233*(1), 26–36.

Skrivergaard, S., Jensen, M. S., Rolander, T. B., Nguyen, T. B. N., Bundgaard, A., Nejsum, L. N., & Martensen, P. M. (2019). The cellular localization of the p42 and p46 oligoadenylate synthetase 1 isoforms and their impact on mitochondrial respiration. *Viruses*, *11*(12). https://doi.org/10.3390/v11121122

Soult, M. C., Lonergan, N. E., Shah, B., Kim, W. K., Britt, L. D., & Sullivan, C. J. (2013). Outer membrane vesicles from pathogenic bacteria initiate an inflammatory response in human endothelial cells. *Journal of Surgical Research*, *184*(1), 458–466. https://doi.org/10.1016/j.jss.2013.05.035

Teixeira, L. D., Harrison, N. A., da Silva, D. R., Mathews, C. E., Gonzalez, C. F., & Lorca, G. L. (2022). Nanovesicles from *Lactobacillus johnsonii* N6.2 reduce apoptosis in human beta cells by promoting AHR translocation and IL10 secretion. *Frontiers in Immunology*, *13*, 899413. https://doi.org/10.3389/fimmu.2022.899413

Valladares, R., Sankar, D., Li, N., Williams, E., Lai, K. K., Abdelgeliel, A. S., Gonzalez, C. F., Wasserfall, C. H., Larkin, J., Schatz, D., Atkinson, M. A., Triplett, E. W., Neu, J., & Lorca, G. L. (2010). *Lactobacillus johnsonii* N6.2 mitigates the development of type 1 diabetes in BB-DP rats. *PLoS ONE*, *5*(5), e10507. https://doi.org/10.1371/journal.pone.0010507

Wakatsuki, T., Schwab, B., Thompson, N. C., & Elson, E. L. (2001). Effects of cytochalasin D and latrunculin B on mechanical properties of cells. *Journal of Cell Science*, *114*(5), 1025–1036. https://doi.org/10.1242/jcs.114.5.1025

Wang, X., Eagen, W. J., & Lee, J. C. (2020). Orchestration of human macrophage NLRP3 inflammasome activation by *Staphylococcus aureus* extracellular vesicles. *Proceedings of the National Academy of Sciences*, *117*(6), 3174–3184.

Wang, L., Nie, J., Sicotte, H., Li, Y., Eckel-Passow, J. E., Dasari, S., Vedell, P. T., Barman, P., Wang, L., Weinshiboum, R., Jen, J., Huang, H., Kohli, M., & Kocher, J. P. A. (2016). Measure transcript integrity using RNA-seq data. *BMC Bioinformatics*, *17*(1), 1–16. https://doi.org/10.1186/s12859-016-0922-z

Wickenhagen, A., Sugrue, E., Lytras, S., Kuchi, S., Noerenberg, M., Turnbull, M. L., Loney, C., Herder, V., Allan, J., Jarmson, I., Cameron-Ruiz, N., Varjak, M., Pinto, R. M., Lee, J. Y., Iselin, L., Palmalux, N., Stewart, D. G., Swingler, S., Greenwood, E. J. D., … Wilson, S. J. (2021). A prenylated dsRNA sensor protects against severe COVID-19. *Science*, *374*(6567), eabj3624. https://doi.org/10.1126/science.abj3624

SUPPORTING INFORMATION

Additional supporting information can be found online in the Supporting Information section at the end of this article.

How to cite this article: da Silva, D. R., Gonzalez, C. F., & Lorca, G. (2023). Internalization of extracellular vesicles from *Lactobacillus johnsonii* N6.2 elicit an RNA sensory response in human pancreatic cell lines. *Journal of Extracellular Biology*, *2,* e101. https://doi.org/10.1002/jex2.101